A PLANAR 3 DOF SAMPLE MANIPULATOR FOR NANO-SCALE CHARACTERIZATION

B.R. de Jong[1], D.M. Brouwer[2], H.V. Jansen[1], M.J. de Boer[1], T.G. Lammertink[3], S. Stramigioli[3] and G.J.M. Krijnen[1]

[1]MESA+ Institute for Nanotechnology, [2]Drebbel Institute for Mechatronics, [3]Impact Institute for Mechanics Processes and Control, University of Twente, The Netherlands

ABSTRACT

We present the first monolithic manipulator for in-plane positioning in three degrees of freedom (DOF), based on a parallel flexure-mechanism. The manipulator stage is capable of translation in the x- and y-direction (maximum of ±9 µm) as well as rotation about the z-axis (maximum of ±2 degrees). A power-port based model has been developed to give insight in the systems behavior. The effect of anisotropy in the Young's modulus of single crystalline silicon (SCS) on the flexure stiffness is modeled and matches the real system.

1. INTRODUCTION

In the fast growing field of nano-technology, nano-scale characterization is based either on probing techniques (like AFM, STM and MFM) or electron microscopy (SEM and TEM). To facilitate the ever increasing demands for precision and stability of these characterization methods, there is a need for robust, thermally stable, precision manipulators capable of positioning over several microns with nanometer-scale resolution.

Recently, a two DOF manipulator is presented, which is fabricated with the same technology as used in this work [1]. Other groups reported about 2 DOF manipulators allowing one translation or rotation combined with one tilt rotation as well as 3 DOF manipulators capable of three translations [2, 3]. [4] reports about multi DOF manipulators not using flexures but hinges.

Here a parallel mechanism is presented. In such mechanisms, position-errors do not accumulate like in stacked or serial mechanisms. Unlike serial mechanisms, in parallel mechanisms each actuator directly drives the end-effector without another actuation-frame in between. This concept also facilitates simple electrical interconnect. The difference is illustrated in Fig. 1 for a serial and parallel 3 DOF-mechanism.

The use of flexures is preferred over hinges, because hinges with play in the nanometer range are hard if not impossible to realize in MEMS. As a result of play, nano-resolution will certainly not be possible. Furthermore, friction will cause positioning problems due to virtual play. For robustness against bugling, the flexures suspending the platform are re-inforced.

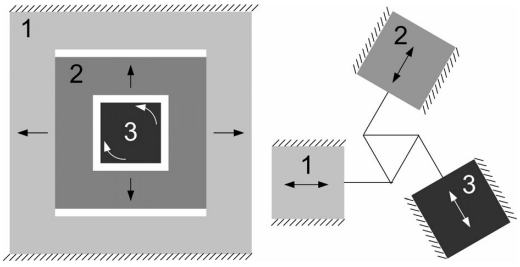

Figure 1. Schematic representation of a serial (left) and a parallel (right) mechanism for 3 DOF planar positioning.

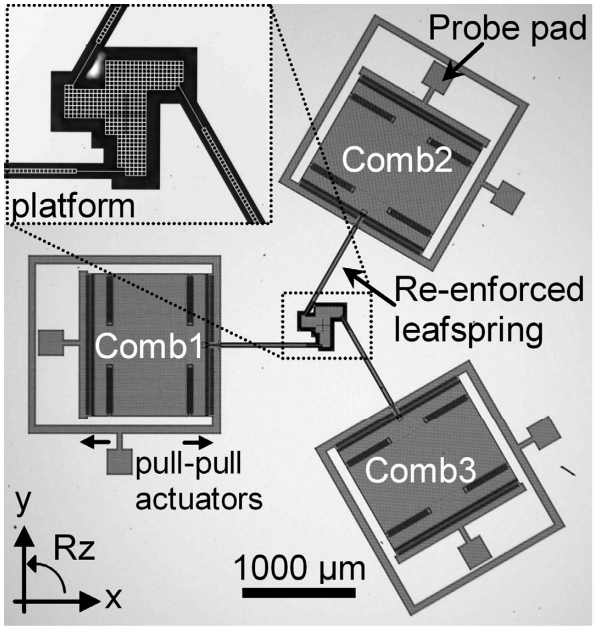

Figure 2. Optical microscope image of the 3 DOF planar manipulator.

The small size of MEMS is beneficial with respect to thermal stability, since the absolute change in length induced by temperature variation is smaller for small sized objects. Especially the design is an important factor in thermal stability. Fig. 2 shows a microscope image of the planar 3 DOF manipulator. The mechanism is symmetrically designed. Assuming a near-symmetric temperature profile, a symmetric design improves thermal stability. The design largely avoids cases of stress build-up that result in non-linear behavior and the flexure mechanism is fabricated in bulk SCS so hardly any mechanical hysteresis is expected. Accurate positioning in both translation and rotation is facilitated by many aspects of the design.

Section 2 will explain positioning with this parallel mechanism. The fabrication process is briefly shown in section 3. In section 4 measurement results are discussed and a comparison is made with a power-port based model. Conclusions and discussion follow in section 5.

2. THEORY

The kinematic concept is shown in Fig 3. An equilateral triangular platform can be moved in-plane (x,y,R_z) by three

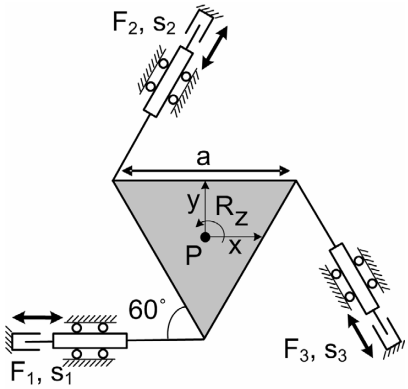

Figure 3. Schematic representation of the parallel kinematic mechanism.

identical actuators. The actuators are connected to the platform by struts, which in reality will be flexure beams.

To develop insight in the mechanism a linear (first order) model of the kinematics is derived. The orientation of tangential direction for the actuator strokes is chosen with s_1 along the x-axes. Because of the parallel kinemetic mechanism, the strokes s_i do not (necessarily) correspond to orthogonal coordinates (x,y,R_z). To find the correspondence, use is made of inverse kinematics. A displacement of point P along the coordinates is assumed and the necessary strokes are calculated. Likewise, the transformation matrix is derived and can be used in the following formula:

$$\begin{bmatrix} s_1 \\ s_2 \\ s_3 \end{bmatrix} = \begin{bmatrix} 1 & 0 & \frac{\sqrt{3}a}{3} \\ -\frac{1}{2} & -\frac{\sqrt{3}}{2} & \frac{\sqrt{3}a}{3} \\ -\frac{1}{2} & \frac{\sqrt{3}}{2} & \frac{\sqrt{3}a}{3} \end{bmatrix} \begin{bmatrix} x \\ y \\ R_z \end{bmatrix} \; inv \rightarrow \begin{bmatrix} x \\ y \\ R_z \end{bmatrix} = \begin{bmatrix} \frac{2}{3} & -\frac{1}{3} & -\frac{1}{3} \\ 0 & -\frac{\sqrt{3}}{3} & \frac{\sqrt{3}}{3} \\ \frac{1}{\sqrt{3}a} & \frac{1}{\sqrt{3}a} & \frac{1}{\sqrt{3}a} \end{bmatrix} \begin{bmatrix} s_1 \\ s_2 \\ s_3 \end{bmatrix}$$

The inverse of the transformation matrix gives the relations between the movements along coordinates (x,y,R_z) and the strokes s_i. It should be stressed that the transformation matrix is only valid in point P. However, since in the MEMS device flexures are used, strokes will be limited and very small compared to the device dimensions. Therefore this linearization serves well enough to characterize the kinematics of the manipulator.

3. FABRICATION PROCESS

The simple 2-maks process (see Fig. 4) is based on bulk micromachining of conventional <100> P^+ Si wafers in combination with trench isolation [1]. First, trenches are etched with the Bosch process (Alcatel Adixen 100SE) and refilled with isolating LPCVD silicon-rich-nitride (SiRN). These will later form electrical isolated regions in the Si. Second, mechanical structures are etched and released sequentially in one and the same dry-etch reactor. The first phase is etching of etch-holes with the Bosch process. In the second phase, the structures are released by dry isotropic etching. This process enables structures of 40 µm in height, being mechanically connected while electric isolated, without the need for SOI wafers. The height of the structures largely increases the robustness of the system. Dry release is invulnerable to sticking.

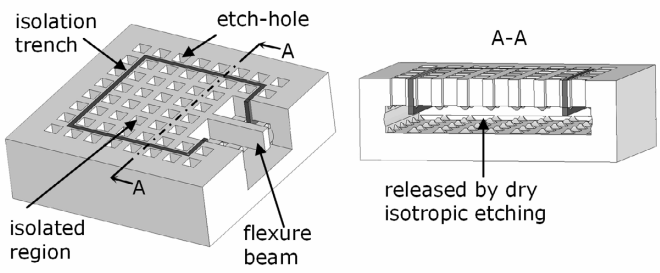

Figure 4. 3D schematic overview of process features (left), cross-section over A-A (right).

4. RESULTS

The complete system is shown in Fig. 1 and 6. Each corner of the platform is connected to a *pull-pull* combdrive via a re-inforced flexure. Driving voltages can be applied via the probe pads. The pads are electrically connected to the combteeth via leads consisting of the electrically isolated regions as shown in Fig. 4. The shuttles of the combdrives are electrically connected to the bulk through "folded flexures". The bulk is used as electrical ground connection.

Measurements

To verify if the system behaves as expected, voltages are applied in the ratios following from the transformation matrix (assuming $s_i(V_i)$ linear and equal for all i). For example to move purely in the x-direction the relation between V_1, V_2 and V_3 is (keeping in mind the quadratic relation between voltage and force).

$$V_2 = V_3 = \frac{V_1}{\sqrt{2}}$$

Combdrives 2 and 3 are driven in opposite direction to combdrive 1. Like this the platform is driven in pure x and y direction and rotation about the z axis. At various voltage values, pictures were taken of the platform. Displacements and rotations are measured with pattern-matching based on correlation. Testing this method on a fixed distance results in a standard deviation of 0.07 µm for translations and 0.02° for rotation. These are assumed to be the measurement errors.

Fig. 5 a, b and c show measurement results for translations in x and y direction and rotation about the z-axis respectively. The horizontal axis represents the squared voltage applied to combdrives (V_1 for the x direction). A negative value for the squared voltage means movement in the opposite direction. The graphs show linear trend-lines for the translations and rotation. The behavior of the system is expected to be linear with the squared actuation voltage.

The difference between the measured values and the trend-lines is within standard deviation (the y translation shows combdrive flexure stiffening at the maximum displacement). The platform also returns to its zero position within 0.07 µm, so hysterisis is not detected. This is in agreement with expectations. More precise measurement techniques – like Fourier spectrum matching – need to be

used in future to characterize the system up to nanometer level.

Fig. 5 a and b also show cross-talk in translation. Small changes in the platform orientation are also detected during translation and small displacements are found during rotation. Furthermore, the ratio of displacement in x and y direction for the same driving voltage is found to be 0.81. The inverse kinematic model predicts a ratio of $\frac{1}{2}\sqrt{3} \approx 0.87$. These deviations occur because the assumption for the driving voltages does not hold. There are two reasons why the system does not correspond to the inverse kinematic model. First the dimensions are not exactly according to the model and second the model does not take into account stiffness and non-linearity. Stiffness of flexures in bulk <100> SCS depends not only on dimensions but also on orientation. The Young's modulus of SCS is anisotropic. Along the <100> direction the Young's modulus is 130 GPa while 60˚ with respect to this direction it is 158 GPa [5].

Fig. 6 shows a SEM micrograph of the platform, its suspension and part of the combdrives. Some places of specific interest are marked. From these areas pictures are taken at much larger magnification. Mark 1 and 2 show parts of the thin section of the re-inforced flexures suspending the platform. Mark 3 and 4 show details of the comb-teeth. The flexure widths (2 µm by design) of 1 and 2 are not equal and 2 shows a profile in the beam width. This profile is also visible in the comb-teeth of 4. The reason for this profile resides in the way the photo-lithography masks are written. A laser writes dots and scans the mask. Features along the scan-direction are written according to design, but those under an angle unequal to 90˚ to the scan direction show aliasing. Marks 2 and 4 are under an angle of 60˚, hence the profile. For the flexures this means a different stiffness than expected and than can be calculated for a rectangular profile.

In order to extract more data about the flexure stiffness, forced harmonic excitations in x, y and Rz direction are applied. These will excite linear combinations of pure modes of the system. By visual inspection the first amplitude maximum was found for x, y and Rz. Because of the quadratic relation between driving voltage and displacement, the corresponding driving frequency needs to be doubled to obtain the frequency of the movement. The frequencies found, are listed in Table 1.

Table 1. Frequencies from measurements and model.

f [Hz]	x-translation	y-translation	Rz-rotation
measured	1200 ± 4	1160 ± 4	1457 ± 4
model	1190	1176	1333

Modeling

A dynamic power-port based model in *20-sim 3.6* is used to obtain more insight in the behavior of the system. In this model, multidimensional stiffness-elements can be defined which are handled as energy buffers. Active elements in the model are connected through power flows. The difference in stiffness due to the anisotropic Young's modulus is taken into account and an attempt is made to model the effect of

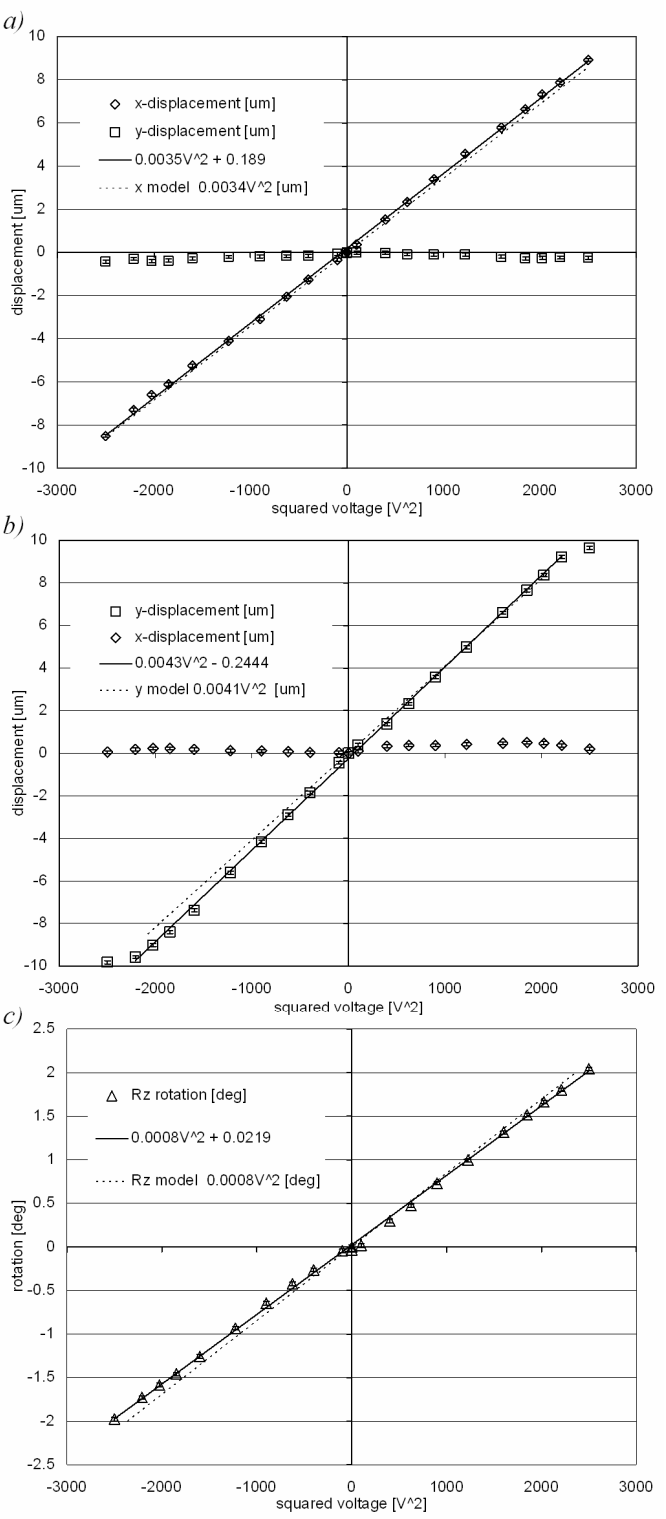

Figure 5. Graphs of x-displacement (a), y-displacement (b) and rotation about the z-axis (c) against the squared driving voltage.

the profile in the flexure width. The height of the structures is obtained from SEM images and amounts to 38 µm.

For the dynamic model, values for the stiffness of the combdrive suspension and the re-inforced flexures are needed. The total stiffness of the "folded flexure" combdrive suspension in the direction of the stroke is calculated by [6]:

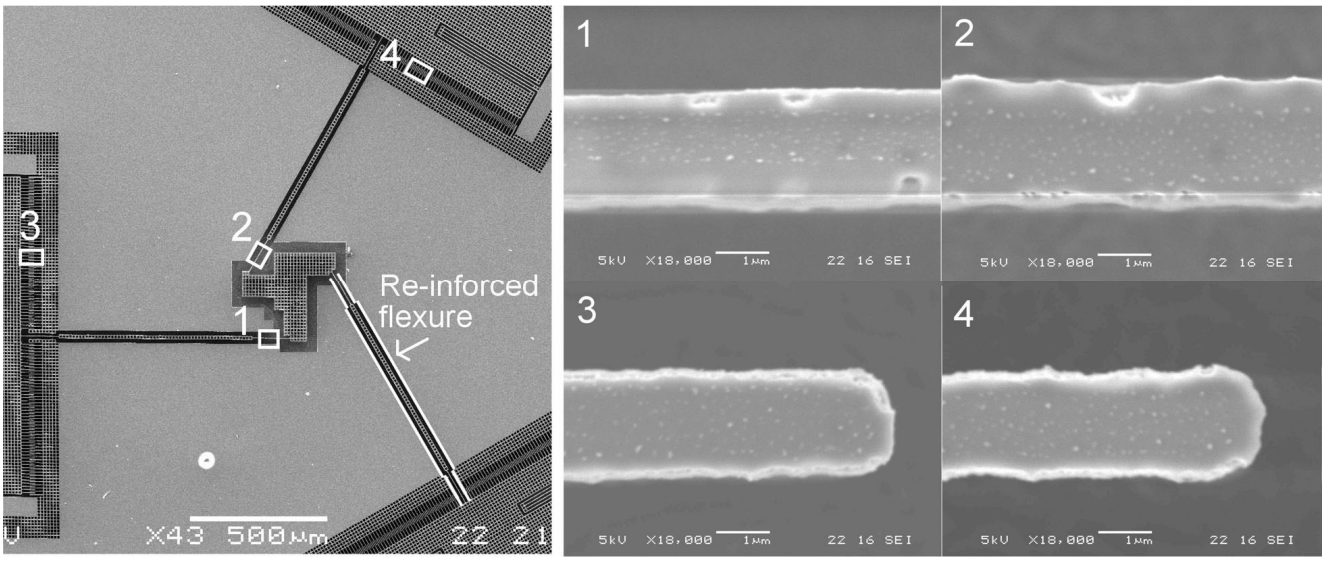

Figure 6. SEM micrograph of the platform with suspension (left), and four details (right).

$$K_{cs} = \frac{48EI}{l_{cs}}$$

Where E [Pa] is the Young's modulus, I [m^4] is the moment of inertia and l_{cs} is the length of one beam of a flexure. The re-inforced flexures are modeled with stiffness in 3 DOF (in-plane rotation $d\varphi$, lateral translation du, longitudinal translation dv), resulting in a stiffness matrix evaluated at the end of the flexure:

$$\begin{bmatrix} M_\varphi \\ F_u \\ F_v \end{bmatrix} = \begin{bmatrix} \frac{(p^2+p+4)EI}{L(1-p^3)} & \frac{-6EI}{L^2(1-p^3)} & 0 \\ \frac{-6EI}{L^2(1-p^3)} & \frac{12EI}{L^3(1-p^3)} & 0 \\ 0 & 0 & \frac{EA}{L(1-p)} \end{bmatrix} \begin{bmatrix} d\varphi \\ du \\ dv \end{bmatrix} \text{ with } p = \frac{L-2l}{L}$$

Where p is the stiffening parameter for the re-enforcement, L [m] is the total length of the flexure and l [m] is the length of each thin part, A [m^2] is the cross-section area of the thin parts. The re-enforcement is considered rigid.

The results of the model for x and y translation and rotation about z are plotted in the graphs of Fig. 5. There is a small deviation from the measurements. It seems the modeled stiffness values are a little too large. Except for the rotation, here they are too small. However, if the frequencies for maximum amplitude for forced excitation of the modeled system are compared with the ones measured, they are in good agreement. Except for the resonance in rotation, where the stiffness seems to be too low again. Furthermore, the ratio between displacement in x and y direction at the same driving voltage is 0.83, which is quite close the ratio of 0.81 of the real system.

5. CONCLUSION AND DISCUSION

A planar, parallel-kinematic 3 DOF manipulator for nano-scale characterization has been presented. An inverse kinemetic model is explained and equations for the flexure suspension are derived. Displacements of the manipulator platform are measured with a sub-pixel correlation method and a dynamic simulation is performed. Variations of the stiffness in different directions in SCS are successfully modeled leading to results that match the behavior of the system reasonably well.

The question remains if the system is suitable for nano-positioning. Important limitations to accurate positioning are non-linear behavior as a result of preferential positions, play, friction and hysteresis and instability of the driving voltage. The design deals with avoiding over-constrained DOFs, play and friction. SCS is a good choice to minimize hysteresis. Judging from these aspects, nano-positioning is in reach. Measurements with nanometer resolution are necessary to further characterize the system. Extensive data of the systems behavior can be used to implement a control system.

Fabrication can be improved concerning the lithography mask. A mask writer with smaller spot size or compensation for aliasing can be used to reduce variations in dimensions related to the orientation of the laser scan direction.

ACKNOWLEDGEMENT

This work has been made possible by the financial support of the Dutch ministry of economic affairs program IOP Precision Technology.

REFERENCES

[1] E. Sarajlic et al., *Transducers 2005,* 2, pp. 302-303
[2] H-Y. Chu, *Transducers 2005, pp. 737-740*
[3] Y-C. Tung and K. Kurabayashi. *Journal of MEMS*, 14 (2005), pp 548-557
[4] B. Jokiel et al., *ASPE Meeting 2001*, 25, pp.32-35
[5] Wortman, J.J., R.A. Evans, *J. Appl. Phys.* 36 (1965), pp. 153-156
[6] R. Legtenberg et al., *Journal of Micromechanics and Microengineering*, 6 (1996), pp. 320-329